Binuclear Manganese(III) Complexes of Potential Biological Significance

John E. Sheats,[1a] Roman S. Czernuszewicz,[1b] G. Charles Dismukes,*[1b] Arnold L. Rheingold,[1c] Vasili Petrouleas,[1d] JoAnne Stubbe,[1e,f] William H. Armstrong,[1f] Robert H. Beer,[1f] and Stephen J. Lippard*[1f]

Contribution from the Departments of Chemistry, University of Delaware, Newark, Delaware 19711, Massachusetts Institute of Technology, Cambridge, Massachusetts 02139, and Princeton University, Princeton, New Jersey 08544, and the Department of Physics, Nuclear Research Center "Demokritos", Athens, Greece. *Received July 14, 1986*

Abstract: The synthesis of several binuclear, oxobis(carboxylato)-bridged dimanganese(III) complexes, $[Mn_2O(O_2CR)_2(HB(pz)_3)_2]$ where R = CH_3 (**1**), C_2H_5 (**2**), or H (**3**), and $HB(pz)_3^-$ is the hydrotris(1-pyrazolyl)borate ligand, is described. X-ray structural studies of **1**·CH_3CN and **1**·4CH_3CN reveal two six-coordinate manganese atoms bridged by a μ-oxo [av Mn–O, 1.78 Å; Mn–O–Mn, 125.1°] and two μ-acetato (av Mn–O, 2.07 Å) groups and capped by two tridentate $HB(pz)_3^-$ ligands. Each high spin, d^4 Mn(III) center has its empty d-orbital directed toward the short $Mn–O_{oxo}$ bond axis, the consequences of which are a shortening of Mn–N bonds trans to the μ-oxo group and markedly reduced antiferromagnetic coupling of the two Mn(III) centers compared to the two high spin, d^5 Fe(III) centers in the $[Fe_2O(O_2CCH_3)_2(HB(pz)_3)_2]$ analogue. In the latter, the spin exchange coupling constant $J = -121$ cm^{-1}, whereas χ_M vs. T measurements over the range $4.2 < T < 300$ K for **1** reveal a J value of ~ -0.5 cm^{-1}. The greater paramagnetism and rapid spin relaxation of the manganese complexes leads to large isotropic shifts and narrow lines in their proton NMR spectra. All protons were observed in the 67 to −56 ppm region, and most could be assigned on the basis of deuterium substitution. The methyl resonance of the bridging acetate ligands in **1** occurs at +65.6 ppm, which should be useful for identifying the $\{Mn_2O(O_2CCH_2R)_2\}^{2+}$ core in biology. These results suggest that substitution of Mn(III) for Fe(III) in metalloproteins such as hemerythrin or ribonucleotide reductase, that are known or believed to contain such cores, would provide a powerful NMR structural probe. The results of UV–vis, Raman, and infrared spectral studies are reported, including work on isotopically substituted **1**, from which the symmetric and asymmetric Mn–O–Mn bridge bond stretching frequencies are assigned at 558 and 717 cm^{-1}, respectively. Electrochemical studies of **1** reveal a quasi-reversible one-electron oxidation at 0.51 V vs. the Fc^+/Fc couple to form the mixed valence Mn_2(III,IV) complex. The ESR spectrum of a species, which was chemically generated from **1**, exhibits a 16-line ^{55}Mn hyperfine pattern that is typical of the Mn_2(III,IV) trapped valence state. This spectrum closely matches that observed for the 300 K form of the S_2 state of the manganese complex involved in photosynthetic water oxidation in green plants. Further oxidation of the mixed valence species reveals a second, quasi-reversible wave at 1.22 V vs. Fc^+/Fc, tentatively assigned as the Mn_2(IV,IV) complex.

Manganese is required in living systems to perform diverse redox functions including water splitting by photosynthetic enzymes,[2] disproportionation of hydrogen peroxide (catalase activity) in microorganisms,[3] and reduction of ribo- to deoxyribonucleotides in coryneform bacteria.[4] As evidence implicating polynuclear centers in several of these enzymes has accumulated, various attempts have been made to prepare and characterize manganese complexes having analogous spectroscopic and magnetic properties.[5] Recently we and others have shown that binuclear iron(III) complexes containing the (μ-oxo)bis(μ-carboxylato)diiron(III) core are good models for the diiron(III) centers in methemerythrin and, most likely, ribonucleotide reductase.[6] It was thus of interest to extend this chemistry to manganese(III) to determine the extent to which the properties of the (μ-oxo)bis(μ-carboxylato)dimanganese(III) center mimic those of the known binuclear manganese enzymes. A recent report described the synthesis, structure, and redox behavior of this binuclear manganese(III) center in $[Mn_2O(O_2CCH_3)_2(TACN)_2]^{2+}$, where TACN = 1,4,7-triazacyclononane.[7] Here we describe our independent studies of the hydrotris(1-pyrazolyl)borate analogues, $[Mn_2O(O_2CR)_2(HB(pz)_3)_2]$, which considerably sharpen our understanding of this interesting binuclear manganese(III) core and delineate the relevance of its properties to those of the known polynuclear manganese centers in biology.

Experimental Section

Preparation of Compounds. General Methods. Potassium hydrotris(1-pyrazolyl)borate ($KHB(pz)_3$) was prepared by Trofimenko's procedure.[8] ^{18}O-enriched water was purchased from Cambridge Isotope Laboratories, Woburn, MA. "$Mn(O_2CCH_3)_3·2H_2O$" was obtained from Alfa and Aldrich. Acetonitrile was distilled from CaH_2. All other chemicals were obtained from commercial sources in highest available purity. Elemental analyses were performed by Galbraith Laboratories, Knoxville, TN or by Atlantic Microlab, Atlanta, GA.

(μ-Oxo)bis(μ-acetato)bis(hydrotris(1-pyrazolyl)borato)dimanganese(III), $[Mn_2O(O_2CCH_3)_2(HB(pz)_3)_2]$ (1). Method A. To 50 mL of glacial acetic acid was added 2.50 g (10.2 mmol) of $Mn(O_2CCH_3)_2·4H_2O$ and 0.81 g (5.1 mmol) of $KMnO_4$. The solution was heated to 80 °C for 45 min with stirring, filtered, and allowed to cool to room temperature. During this period the solution turned from purple to chocolate brown.

(1) (a) National Science Foundation Small College Faculty Fellow, Princeton University, summers 1984 and 1985; permanent address: Rider College, Lawrenceville, NJ 08648. (b) Princeton University. (c) University of Delaware. (d) Nuclear Research Center "Demokritos". (e) National Institutes of Health Research, Career Development Awardee, MIT, 1984–5; permanent address: Department of Biochemistry, University of Wisconsin, Madison, WI 53706. (f) Massachusetts Institute of Technology.

(2) For leading references, see: (a) Dismukes, G. C. *Photochem. Photobiol.* **1986**, *43*, 99. (b) dePaula, J. C.; Brudvig, G. W. *J. Am. Chem. Soc.* **1985**, *107*, 2643. (c) Kirby, J. A.; Robertson, A. S.; Smith, J. P.; Thompson, A. C.; Cooper, S. R.; Klein, M. P. *J. Am. Chem. Soc.* **1981**, *103*, 5529.

(3) (a) Kono, Y.; Fridovich, I. *J. Biol. Chem.* **1983**, *258*, 6015, 13646. (b) Beyer, W. F., Jr.; Fridovich, I. *Biochemistry* **1985**, *24*, 6460.

(4) (a) Schimpff-Weiland, G. S.; Follmann, H.; Auling, G. *Biochem. Biophys. Res. Commun.* **1981**, *102*, 1276. (b) *Thioredoxin and Glutaredoxin Systems*; Holmgren, A., Bränden, C.-I., Jörnvall, H., Sjöberg, B.-M., Eds.; Raven Press: New York, 1986; pp 217–226.

(5) (a) Cooper, S. R.; Calvin, M. *J. Am. Chem. Soc.* **1977**, *99*, 6623. (b) Cooper, S. R.; Dismukes, G. C.; Klein, M. P.; Calvin, M. *Ibid.* **1978**, *100*, 7248. (c) Lynch, M. W.; Hendrickson, D. N.; Fitzgerald, B. J.; Pierpont, C. G. *Ibid.* **1984**, *106*, 2041. (d) Mathur, P.; Dismukes, G. C. *Ibid.* **1983**, *105*, 7093. (e) Unni Nair, B. C.; Dismukes, G. C. *Ibid.* **1983**, *105*, 124. (f) Okawa, H.; Honda, A.; Nakamura, M.; Kido, S. *J. Chem. Soc., Dalton Trans.* **1985**, 59. (g) Vincent, J. B.; Folting, K.; Huffman, J. C.; Christou, G. *Inorg. Chem.* **1986**, *25*, 996.

(6) (a) Armstrong, W. H.; Lippard, S. J. *J. Am. Chem. Soc.* **1983**, *105*, 4837. (b) Wieghardt, K.; Pohl, K.; Gebert, W. *Angew. Chem., Int. Ed. Engl.* **1983**, *22*, 727. (c) Armstrong, W. H.; Spool, A.; Papaefthymiou, G. C.; Frankel, R. B.; Lippard, S. J. *J. Am. Chem. Soc.* **1984**, *106*, 3653. (d) Lippard, S. J. *Chem. Britain* **1986**, 222.

(7) Wieghardt, K.; Bossek, V.; Ventur, D.; Weiss, J. *J. Chem. Soc., Chem. Commun.* **1985**, 347.

(8) Trofimenko, S. *Inorg. Synth.* **1970**, *12*, 99.

0002-7863/87/1509-1435$01.50/0

After the addition of 2.50 g (9.92 mmol) of $K(HB(pz)_3)$ the solution was stirred for 15 min, filtered, and evaporated to dryness in vacuo with heating up to 60 °C. The glassy brown residue was dissolved in CH_2Cl_2 and filtered to remove a tan residue. Removal of the solvent in vacuo gave a purple residue which was dissolved in 25–50 mL of CH_2Cl_2, filtered, diluted with 5 times its volume of CH_3CN, and allowed to stand for 3 h at room temperature, then subsequently for 24–48 h at −5 °C. Deep purple prisms were isolated, 2.2 g (62% yield, assuming one CH_3CN molecule of crystallization). After concentration the mother liquor yielded a second crop, 0.5 g (14%), of less pure material. A portion of the first crop was finely ground and dried at 60 °C in vacuo overnight. Anal. Calcd for $Mn_2O_5N_{12}C_{22}B_2H_{26}$ (**1**): C, 39.44; H, 3.91; N, 25.09; Mn, 16.40. Found: C, 39.44; H, 4.01; N, 25.19; Mn, 15.93.

Method B. A 1.0-g (4.0 mmol) portion of $K(HB(pz)_3)$ in 5 mL of dry CH_3CN was added to a solution of 1.02 g (3.8 mmol) of manganese(III) acetate dihydrate in 96 mL of degassed CH_3CN. The reaction mixture was heated to 65 °C under nitrogen for 75 min, cooled to room temperature, and filtered to remove 0.57 g of a brown solid. Solvent was removed from the filtrate under vacuum to form a purple-black residue which was triturated with ~60 mL of cold ether. Filtration and drying in air afforded 0.88 g (66%) of a purple solid which was recrystallized to give 0.47 g (35%, assuming one CH_3CN molecule of crystallization) of product: IR (KBr, cm^{-1}), 3198, 3126, 3119, 2479 (BH), 1580, 1504, 1407, 1391, 1343, 1311, 1212, 1118, 1113, 1091, 1070, 1047, 987, 975, 928, 881, 816, 789, 760, 712, 666, 659, 617, ~540 (br). Anal. Found: C, 39.69; H, 4.07; N, 25.06.

Both types of crystals, **1**·4CH_3CN and **1**·CH_3CN, used for X-ray diffraction studies (see below) lose solvent readily in vacuo. Selectively deuteriated **1** was prepared according to method A either by using $Na(DB(pz)_3)$ or NaO_2CCD_3 as described previously for the iron(III) analogues.[6c] A sample containing ^{18}O selectively substituted into the bridging position was also made under nitrogen as described for the iron analogue[6c] except that the exchange reaction mixture was stirred for only 15–30 min to avoid decomposition and the formation of a brownish black precipitate. The mass spectrum of the purple flakes (product) showed a parent ion peak shift from 670 to 672.

(μ-Oxo)bis(μ-propionato)bis(hydrotris(1-pyrazolyl)borato)dimanganese(III), $[Mn_2O(O_2CC_2H_5)_2(HB(pz)_3)_2]$ (2). This compound was prepared by method A used for **1** except that propionic acid was used as solvent, and no precipitate formed: yield, 3.15 g (91%) of shiny purple crystals. IR (KBr, cm^{-1}) 3140, 3122, 2970, 2938, 2879, 2480 (BH), 1729 (w), 1580, 1501, 1465, 1403, 1390, 1370, 1310, 1212, 1112, 1071, 1049, 987, 975, 922, 882, 814, 790, 757, 715, 658, 620, 550 (br), 360, 340. Anal. Calcd for $Mn_2O_5N_{12}C_{24}B_2H_{30}$ (**2**): C, 41.29; H, 4.33; N, 24.08; Mn, 15.74. Found: C, 41.26; H, 4.50; N, 24.03; Mn, 15.67.

(μ-Oxo)bis(μ-formato)bis(hydrotris(1-pyrazolyl)borato)dimanganese(III), $[Mn_2O(O_2CH)_2(HB(pz)_3)_2]$ (3). This compound was prepared by ligand exchange by analogy to reaction chemistry reported for the iron(III) analogue.[9] A solution of 0.335 g (0.5 mmol) of **1** in 25 mL of CH_2Cl_2 was stirred for 1.5 h with 25 mL of 1.0 M HCO_2H/1.0 M $NaHCO_3$ in water at room temperature. The methylene chloride layer was separated, washed with distilled water, and filtered, and the solvent was evaporated. The crude product was recrystallized from ~12 mL of 1:5 CH_2Cl_2/CH_3CN at −5 °C to yield 100 mg (31%) of purple needles. IR (KBr, cm^{-1}) 3120, 2920, 2850, 2480 (BH), 1597, 1503, 1405, 1390, 1350, 1312, 1212, 1113, 1048, 980, 760, 713, 660, 530 (br), 368, 338. Anal. Calcd for $Mn_2O_5N_{12}C_{20}B_2H_{23}$: C, 37.42; H, 3.45; N, 26.18; Mn, 17.12. Found: C, 37.77; H, 3.65; N, 25.86; Mn, 16.87.

CAUTION. One of us has experienced an allergic reaction to compound **1** and suitable care should be taken to avoid contact with it and its analogues either in solution or as dust.

Collection and Reduction of X-ray Data. $[Mn_2O(O_2CCH_3)_2(HB(pz)_3)_2]$·4$CH_3CN$ (1·4CH_3CN). Deep red-purple truncated square pyramidal crystals of **1**·4CH_3CN, obtained by cooling a saturated solution of **1** in dry CH_3CN to 0 °C, were mounted at low temperature on the end of a glass fiber with silicone grease and rapidly transferred to the cold stream (−65 °C) of the diffractometer to prevent solvent loss. Open counter ω scans showed no structure and acceptable peak widths, $\Delta\omega_{1/2}$ ~ 0.2°. Study on the diffractometer showed the crystal to be isomorphous with its iron analogue, $[Fe_2O(O_2CCH_3)_2(HB(pz)_3)_2]$·4$CH_3CN$, **4**·4$CH_3CN$,[6c] belonging to space group $P2_1/n$ (C_{2h}^5, No. 14 in a nonstandard setting).[10a] Data collection and reduction were carried out by using procedures described previously,[11] details of which are given in Table I along with the crystal parameters.

Table I. Experimental Details of the X-ray Diffraction Studies of $[Mn_2O(O_2CCH_3)_2(HB(pz)_3)_2]$ (**1**) for **1**·4CH_3CN and **1**·CH_3CN[a]

	1·4CH_3CN	**1**·CH_3CN
	(A) Crystal Parameters	
a, Å	13.115 (3)	19.162 (2)
b, Å	15.097 (6)	19.162 (2)
c, Å	21.662 (5)	53.547 (8)
β, deg	107.26 (2)	120
vol, Å^3	4088.3	17027
space group	$P2_1/n$	$R\bar{3}c$
Z	4	18
ρ (calcd) g cm^{-3}	1.355	1.248
mol wt	834.2	711.1
T (K)	208	295
	(B) Measurement and Treatment of Intensity Data	
instrument	Enraf-Nonius CAD-4F diffrctmtr	Nicolet R3 diffrctmtr
radiation	Mo Kα (λ 0.7107 Å)	Mo Kα (λ 0.7107 Å)
data collected	10245	6153
unique data used	5841	2109
	$F > 4\sigma(F)$	$F > 3\sigma(F)$
	(C) Final Model in Least Squares Refinement	
final R values	R_1 = 0.041	R_1 = 0.071
	R_2 = 0.049	R_2 = 0.075
largest peak on final diffrnc map, e/Å^3	0.30	0.97

[a] $R_1 = \sum||F_o| - |F_c||/\sum|F_o|$; $R_2 = [\sum w(|F_o|^2 - |F_c|^2)/\sum w|F_o|^2]^{1/2}$.

$[Mn_2O(O_2CCH_3)_2(HB(pz)_3)_2]$·$CH_3CN$ (1·CH_3CN). Purplish-brown rectangular plates of **1**·CH_3CN isolated directly from the 4:1 CH_3CN:CH_2Cl_2 mother liquor (method A) at 0 °C were mounted on a glass fiber and coated with epoxy resin to prevent loss of solvent. Study at room temperature on the diffractometer revealed $\bar{3}m$ Laue symmetry and systematic absences consistent with either space group $R3c$ (C_{3v}^6, No. 161) or $R\bar{3}c$ (D_{3d}^6, No. 167).[10b] The latter was favored by statistical tests and confirmed by the successful solution and refinement of the structure. Further details of the data collection and reduction are given in Table I.

Structure Solution and Refinement. $[Mn_2O(O_2CCH_3)_2(HB(pz)_3)_2]$·4$CH_3CN$ (1·4CH_3CN). The structure was solved by standard direct and difference Fourier methods. The refinement of the structure, atomic scattering factors used, and assignment of the thermal parameters were the same as described previously for the iron analogue.[6c] Least-squares refinement,[12] minimizing the function $\Sigma w(|F_o| - |F_c|)^2$ where $w = 1.2904/[\sigma^2(F_o) + 0.000\,625(F_o)^2]$, converged to the R factors listed in Table I. The largest ratio of parameter shift to estimated standard deviation in the final cycle of refinement was <0.002, and the largest peak on the final difference Fourier map was 0.30 e Å^{-3}. Final nonhydrogen atom positional parameters are presented in Table II, and selected interatomic distances and angles are listed in Table IV. A listing of observed and calculated structure factors is supplied in Table S1 (Supplementary Material), and final thermal and hydrogen atom positional parameters are given in Table S3.

$[Mn_2O(O_2CCH_3)_2(HB(pz)_3)_2]$·$CH_3CN$ (1·CH_3CN). The structure was solved by the direct methods routine and difference Fourier syntheses of the SHELXTL program package.[13] All non-hydrogen atoms were given anisotropic thermal parameters while hydrogen atoms were included as fixed isotropic contributions at d(C–H, B–H) = 0.96 Å. The weighting scheme used in the least-squares refinement was $w = 1.0/[\sigma^2(F_o) + 0.0046(F_o)^2]$, and the largest ratio of parameter shift to esd in the final refinement cycle was 0.027. The final difference Fourier map showed no residual electron density in excess of 0.97 e Å^{-3}; R factors are given in Table I. The final atomic positional parameters are presented in Table III, and selected bond distances and angles are given in Table IV. Table S2 gives observed and calculated structure factors, and final thermal parameters for all atoms together with hydrogen atom fixed positional parameters are included in Table S4.

Physical Measurements. Electrochemistry. Cyclic voltammetry (CV) experiments were performed with a Princeton Applied Research Model 173 potentiostat and a Model 175 universal programmer. CV data were recorded on a Houston Instruments Model 2000 X-Y recorder. Solutions

(9) Armstrong, W. H.; Lippard, S. J. *J. Am. Chem. Soc.* **1985**, *107*, 3730.
(10) *International Tables for X-ray Crystallography*; D. Reidel: Dordrecht, Holland; 1983; Vol. A.: (a) p 181. (b) pp 522–3 and 538–9.
(11) Silverman, L. D.; Dewan, J. C.; Giandomenico, C. M.; Lippard, S. J. *Inorg. Chem.* **1980**, *19*, 3379.
(12) SHELX-76: Sheldrick, G. M. In *Computing in Crystallography*; Schenck, H., Olthof-Hazekamp, R., von Koningsveld, H., Bassi, G. C., Eds.; Delft University: Delft, The Netherlands, 1978; pp 34–42.
(13) Sheldrick, G. M. Version 4.0, Nicolet XRD Corp., Madison, WI.

Table II. Final Positional Parameters for $[Mn_2O(O_2CCH_3)_2(HB(pz)_3)_2]\cdot 4CH_3CN$ ($1\cdot 4CH_3CN$)[a]

atom	x	y	z
Mn1	−0.07994 (3)	0.04455 (2)	0.24803 (2)
Mn2	0.10904 (3)	0.17410 (3)	0.24776 (2)
O	0.05285 (14)	0.06630 (11)	0.24791 (9)
O11	−0.07929 (16)	0.13077 (13)	0.32102 (10)
O12	−0.15178 (15)	0.13765 (14)	0.17749 (10)
O21	0.04738 (18)	0.22710 (13)	0.31821 (11)
O22	−0.01724 (15)	0.22701 (13)	0.17709 (11)
N11	−0.03392 (18)	−0.06673 (16)	0.31605 (12)
N12	−0.23343 (17)	0.01176 (14)	0.24705 (12)
N13	−0.0995 (18)	−0.06019 (16)	0.17693 (12)
N14	−0.09418 (18)	−0.14279 (15)	0.30477 (13)
N15	−0.26747 (18)	−0.07342 (15)	0.24433 (12)
N16	−0.14969 (18)	−0.13799 (16)	0.18430 (13)
N21	0.2563 (2)	0.13878 (16)	0.31939 (13)
N22	0.18413 (18)	0.29311 (14)	0.24845 (13)
N23	0.19240 (18)	0.13884 (15)	0.17776 (12)
N24	0.35233 (19)	0.16040 (16)	0.31056 (13)
N25	0.28814 (18)	0.29926 (14)	0.25056 (12)
N26	0.29696 (18)	0.16131 (15)	0.18951 (12)
N3	−0.4894 (3)	0.1161 (3)	0.0495 (2)
N4	0.4090 (4)	0.3996 (3)	0.5110 (2)
N5	0.1733 (4)	0.3650 (4)	−0.0188 (2)
N6	0.3587 (4)	0.5955 (3)	1.0144 (2)
C11	0.0429 (3)	−0.0804 (3)	0.37136 (17)
C12	0.0329 (3)	−0.1631 (3)	0.39655 (18)
C13	−0.0546 (3)	−0.2003 (2)	0.35340 (18)
C14	−0.3169 (2)	0.06257 (19)	0.24713 (17)
C15	−0.4045 (2)	0.0104 (2)	0.24483 (19)
C16	−0.3697 (2)	−0.0751 (2)	0.24311 (18)
C17	−0.0729 (3)	−0.0693 (3)	0.12273 (17)
C18	−0.1028 (3)	−0.1503 (3)	0.09495 (18)
C19	−0.1512 (3)	−0.1917 (2)	0.13454 (18)
C21	0.2787 (4)	0.0964 (2)	0.37565 (19)
C22	0.3876 (4)	0.0896 (3)	0.4035 (2)
C23	0.4319 (3)	0.1307 (2)	0.36124 (18)
C24	0.1477 (3)	0.37565 (19)	0.24776 (18)
C25	0.2285 (3)	0.4357 (2)	0.24960 (18)
C26	0.3153 (3)	0.38537 (19)	0.25096 (16)
C27	0.1647 (3)	0.0983 (2)	0.12031 (18)
C28	0.2488 (4)	0.0943 (3)	0.09481 (18)
C29	0.3314 (3)	0.1345 (2)	0.13985 (18)
C31	−0.0228 (2)	0.19754 (18)	0.34137 (15)
C32	−0.0408 (3)	0.2468 (2)	0.39744 (17)
C41	−0.1129 (2)	0.20301 (18)	0.15724 (14)
C42	−0.1864 (3)	0.2584 (2)	0.10519 (17)
C51	−0.4215 (3)	0.0681 (3)	0.05868 (19)
C52	−0.3341 (3)	0.0056 (3)	0.0710 (2)
C61	0.3520 (3)	0.3680 (3)	0.4683 (2)
C62	0.2773 (6)	0.3309 (4)	0.4128 (3)
C71	0.1537 (4)	0.3523 (3)	0.0266 (2)
C72	0.1294 (6)	0.3325 (4)	0.0846 (3)
C81	0.3434 (4)	0.5495 (3)	0.9720 (2)
C82	0.3234 (5)	0.4927 (4)	0.9180 (3)
B1	−0.1887 (3)	−0.1497 (2)	0.24372 (19)
B2	0.3543 (3)	0.2141 (2)	0.25084 (18)

[a] See Figure 1 for atom labeling scheme. Esd's, in parentheses, occur in the last significant figure(s) for each parameter.

were prepared in Burdick & Jackson acetonitrile or methylene chloride used directly from the bottle with 0.1 or 0.2 M tetra-*n*-butylammonium perchlorate (TBAP), recrystallized before use, as supporting electrolyte. A three-electrode configuration was used, comprised of a platinum disk working electrode, a platinum wire auxiliary electrode, and AgCl/Ag (in saturated KCl) or saturated calomel (SCE) as reference electrode. Electrode performance was monitored by observing the ferrocenium/ferrocene (Fc^+/Fc) couple in the working solution. Experiments were carried out at room temperature (~22 °C) under dinitrogen.

Raman Spectroscopy. The Raman spectrum of **2** and its ^{18}O-μ-oxo isotopically substituted derivative were obtained by backscattering from the surface of KCl pellets attached to a cold finger kept at liquid nitrogen temperature.[14] The spectrometer consists of a Spex 1401 double monochromator equipped with a cooled RCA 31034 photomultiplier tube. Spectra were collected digitally by using a DEC MINC II computer. The 4067-Å excitation line was provided by a Spectra Physics Model 171 Kr^+ laser.

Table III. Final Positional Parameters for $[Mn_2O(O_2CCH_3)_2(HB(pz)_3)_2]\cdot CH_3CN$ ($1\cdot CH_3CN$)[a]

atom	x	y	z
Mn	4580.3 (6)	4268.9 (6)	7219.6 (3)
O(1)	4856 (3)	4856 (3)	7500
O(2)	4352 (3)	3236 (3)	7383 (1)
O(3)	3338 (3)	3931 (3)	7238 (1)
N(1)	4294 (4)	3662 (4)	6886 (1)
N(2)	4738 (4)	3993 (4)	6675 (1)
N(3)	4832 (4)	5278 (4)	6999 (1)
N(4)	5235 (4)	5425 (4)	6781 (1)
N(5)	5829 (4)	4571 (4)	7116 (1)
N(6)	6078 (4)	4793 (4)	6876 (1)
C(1)	2971 (4)	4079 (4)	7406 (1)
C(2)	2140 (6)	3906 (8)	7346 (2)
C(3)	3694 (5)	2914 (4)	6821 (1)
C(4)	3768 (6)	2774 (6)	6575 (2)
C(5)	4425 (5)	3455 (5)	6488 (1)
C(6)	4699 (5)	5892 (5)	7036 (1)
C(7)	5058 (5)	6449 (5)	6841 (2)
C(8)	5380 (5)	6128 (5)	6686 (1)
C(9)	6447 (5)	4575 (5)	7230 (2)
C(10)	7077 (5)	4778 (6)	7067 (2)
C(11)	6839 (5)	4944 (5)	6845 (2)
B	5489 (5)	4827 (5)	6687 (2)
Cn(1)	6667	5503 (9)	833
Cc(2)	6667	6110 (10)	833
Cc(3)	6667	6879 (12)	833

[a] See footnote a, Table II. Coordinates are multiplied by 10^4.

Mass Spectra. These were recorded on an A.E.I. MS-9 mass spectrometer.

Nuclear Magnetic Resonance Spectroscopy. ^1H NMR spectra were obtained on a Bruker WM 250 NMR spectrometer.

Optical and Infrared Spectroscopy. Electronic absorption spectra were recorded either with a Perkin-Elmer Lambda 7 instrument, a Hewlett-Packard 8450 UV–vis spectrophotometer, or a Cary 14 or 15 spectrophotometer. Infrared spectra were taken on a Perkin-Elmer 283, Digilab Model 20 FTIR, or Nicolet Model 7199 FTIR spectrometer.

Magnetic Susceptibility Measurements. The solution magnetic susceptibility of **1** in CD_2Cl_2, with benzene as an internal standard, was measured by the Evans technique.[15] Solid samples of pulverized **1** were studied by a SQUID-type susceptometer at 10 kG and independently by a vibrating sample magnetometer from 2.5–20 kG, by using procedures described previously.[6c,16]

Results and Discussion

Synthesis and Ligand Exchange Reactions. The binuclear manganese(III) complex $[Mn_2O(O_2CCH_3)_2(HB(pz)_3)_2]$ (**1**) could be prepared from manganese(III) acetate in acetonitrile by a procedure analogous to that reported previously for the iron(III) analogue, $[Fe_2O(O_2CCH_3)_2(HB(pz)_3)_2]$ (**4**). Compound **1** could also be obtained by generating manganese(III) acetate from excess $KMnO_4$ and $Mn(O_2CCH_3)_2\cdot 4H_2O$ in glacial acetic acid followed by the addition of $K(HB(pz)_3)$ and workup to yield **1**. Excess $KMnO_4$ was found to be necessary in order to remove all of the Mn(II) present, traces of which lead to the formation of $Mn(HB(pz)_3)_2$,[17] which is difficult to separate from the final product. Attempts to use commercial manganese(III) acetate in glacial acetic acid lead to no isolated **1**. Although the propionate analogue **2** was obtained in excellent (91%) yield by using the in situ generation of manganese(III) propionate in propionic acid, it was necessary to use ligand exchange (eq 1) to prepare the

$$\underset{\mathbf{1}}{[Mn_2O(O_2CCH_3)_2(HB(pz)_3)_2]} + 2HCO_2H \rightarrow \underset{\mathbf{3}}{[Mn_2O(O_2CH)_2(HB(pz)_3)_2]} + 2CH_3CO_2H \quad (1)$$

formate derivative **3**. The exchange of bridging carboxylate ligands in this chemistry parallels that reported previously for the binuclear iron(III) analogues.[9] Another parallel between the binuclear

(14) Czernuszewicz, R. S.; Johnson, M. K. *Appl. Spectrosc.* **1983**, *37*, 297.

(15) Evans, D. F. *J. Chem. Soc.* **1959**, 2003.

(16) Christou, G.; Collison, D.; Garner, C. D.; Acott, S. R.; Mabbs, F. E.; Petrouleas, V. *J. Chem. Soc., Dalton Trans.* **1982**, 1575.

(17) Trofimenko, S. *J. Am. Chem. Soc.* **1967**, *89*, 3170.

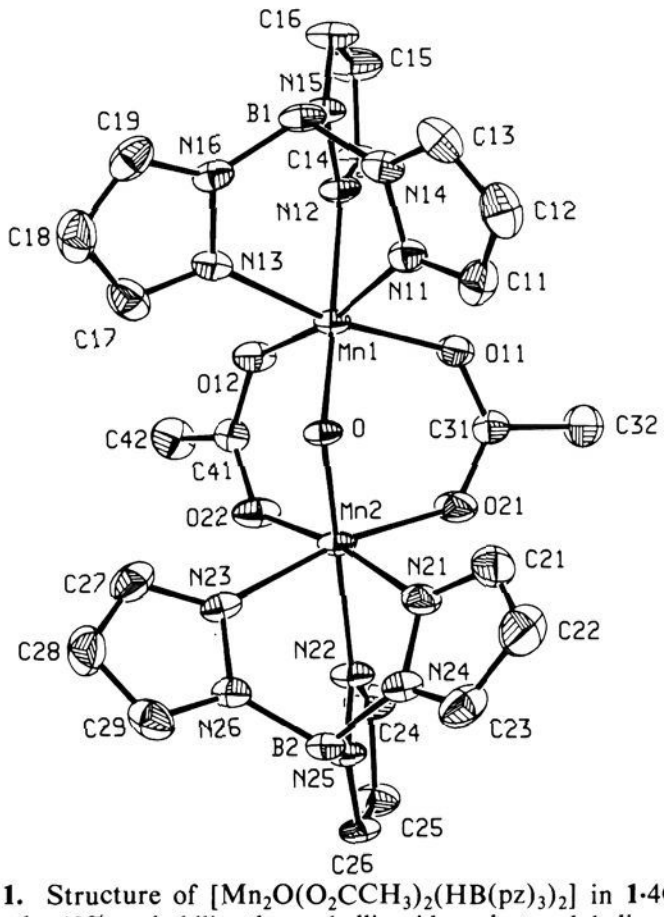

Figure 1. Structure of $[Mn_2O(O_2CCH_3)_2(HB(pz)_3)_2]$ in **1**·4CH_3CN showing the 40% probability thermal ellipsoids and atom labeling scheme.

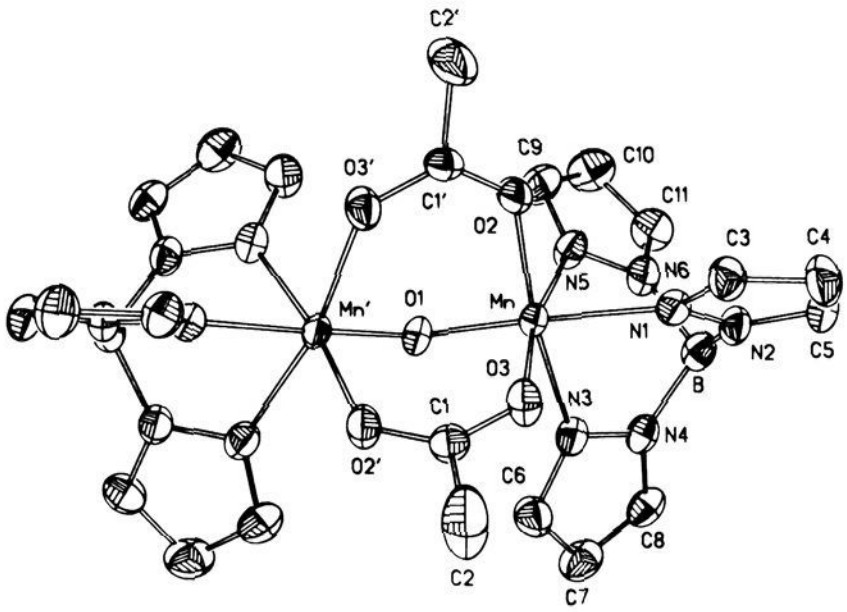

Figure 2. Structure and atom labeling scheme of $[Mn_2O(O_2CCH_3)_2(HB(pz)_3)_2]$ in **1**·CH_3CN displaying the 40% probability thermal ellipsoids.

Mn(III) and Fe(III) systems is the ready exchange of oxygen from water into the bridging, μ-oxo position. These exchange reactions of the bridging ligands in **1** may have possible implications for the ligand exchange chemistry of binuclear manganese centers in biology, although there is presently insufficient knowledge about the latter systems for meaningful comparisons to be made.

Description of the Structure. Figures 1 and 2 display the structure of $[Mn_2O(O_2CCH_3)_2(HB(pz)_3)_2]$ in the **1**·4CH_3CN and **1**·CH_3CN crystalline forms, respectively, from two different perspectives. In the latter crystal form, a twofold symmetry axis passes through the μ-oxo atom relating the two halves of the molecule, while the former has no crystallographically required symmetry. Crystals of compound **1**·4CH_3CN are isomorphous with those of the iron analogue **4**·4CH_3CN. Salient features of the three structures **1**·4CH_3CN, **1**·CH_3CN, and **4**·4CH_3CN are summarized in Table V, together with metrical parameters for the TACN analogues $[M_2O(O_2CCH_3)_2(TACN)_2]^{2+}$, M = Mn (**5**)[7] and Fe(**6**).[6b] From this comparison it is evident that the metal–metal separation, M–O (oxo) distances, and M–O–M angles are in close correspondence for the three hydrotris(1-pyrazolyl)borate complexes and for the two TACN containing complexes. Slight differences occur in the M–O–M bond angles and resultant M···M nonbonded distances between the two series of compounds, however.

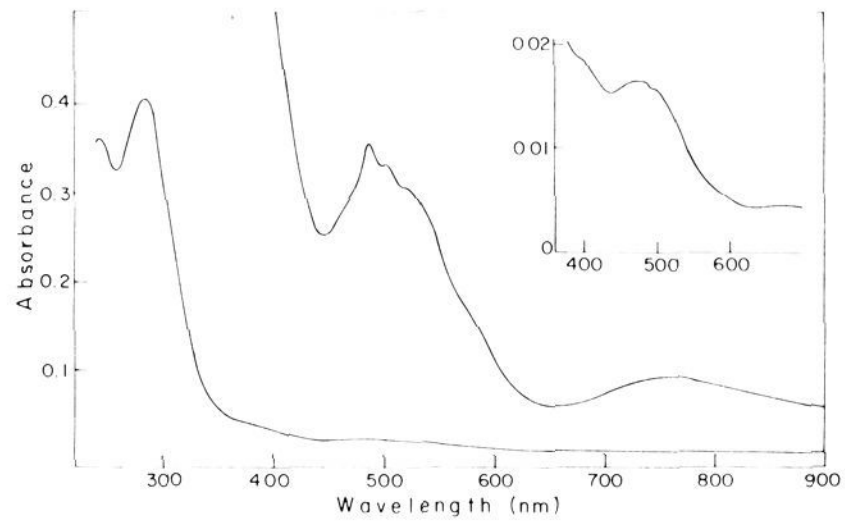

Figure 3. Electronic spectra of $[Mn_2O(O_2CCH_3)_2(HB(pz)_3)_2]$ (**1**) in CH_2Cl_2 and (inset) of the manganese catalase from *L. plantarum*.[3a]

The most noteworthy difference between analogous manganese and iron complexes, **1** vs. **4** and **5** vs. **6**, is that the average Mn–N bond distances trans to the bridging oxo atom are significantly shorter (0.05–0.18 Å) than the cis Mn–N bonds, whereas the Fe–N (trans) bond distances are slightly longer than the Fe–N (cis) bonds (Table V). The pronounced shortening of the trans Mn–N bonds in **1** and **5** may be rationalized as follows. The short Mn–O (oxo) bond raises the energy of the d_{z^2} orbital directed along the Mn–O (oxo) bond vector. This highest lying d-orbital is therefore empty in high spin, d^4 Mn(III), resulting in a shortened trans Mn–N bond. In high spin iron(III), the corresponding d_{z^2} orbital is occupied, and the Fe–N bond is lengthened. This interpretation is further supported by the very different magnetic exchange interactions between metal centers in the iron(III) vs. the manganese(III) complexes (vide infra).

An additional distortion in the metal–ligand geometry of the three manganese complexes listed in Table V is a statistically significant inequivalence of both the Mn–O (carboxylate) and the corresponding trans Mn–N distances. In particular, trans bonds along these O–Mn–N bond axes are either both elongated or both shortened. Such distances which, when combined with the more pronounced N–Mn–O (oxo) bond length effect mentioned above, lead to overall rhombic symmetry at the metal centers, as expected for Jahn–Teller distorted pseudooctahedral d^4 Mn(III) complexes. The significance of this rhombic stereochemistry is underscored by comparison to the results for the Fe(III) analogues, in which the symmetry is tetragonal owing only to the short Fe–O (oxo) bond. Finally, it should be noted that the magnitudes of the rhombic distortions in the two crystalline forms of **1** are not equivalent, the inequivalence in the lengths of the N–Mn–O bond vectors being significantly larger in **1**·CH_3CN than in **1**·4CH_3CN. At present we are uncertain whether this difference results from crystal packing forces, the fact that the X-ray data sets for the two compounds were taken at different temperatures, or both.

Other features of the coordination and ligand geometry of $[Mn_2O(O_2CCH_3)_2(HB(pz)_3)_2]$ in both **1**·CH_3CN and **1**·4CH_3CN are little different from those of the iron analogue **4**·4CH_3CN, which have been discussed in detail elsewhere.[6c]

Electronic Spectra. Figure 3 displays the absorption spectrum of **1** in CH_2Cl_2 together with that published for manganese–catalase of *Lactobacillus plantarum*.[3a] The similarities between these spectra lends support to the notion that the manganese atoms occur as a binuclear unit in this enzyme.[3b] As can be seen from Table VI, both the positions and relative intensities of the absorption maxima for **1** and the manganese–catalase enzyme are comparable. These spectra differ from that[18] of the manganese-containing superoxide dismutase from *Escherichia coli B*, which contains mononuclear Mn(III). Compound **2**, the propionate analogue, has an absorption spectrum (not shown) essentially the same as that of **1**. The spectrum of **1** is similar to that reported for the TACN analogue **5**[7] but is better resolved in the 480–600 nm region.

(18) Keele, B. B., Jr.; McCord, J. M.; Fridovich, I. *J. Biol. Chem.* **1970**, *245*, 6176.

Table IV. Selected Interatomic Distances (Å) and Angles (deg) for $[Mn_2O(O_2CCH_3)_2(HB(pz)_3)_2]\cdot nCH_3CN$, **1**·$nCH_3CN$, n = 4 or 1[a]

	n = 4			n = 1	
Coordination Spheres					
Mn1···Mn2	3.159 (1)	Mn2–O	1.787 (2)	Mn···Mn′	3.175 (1)
Mn1–O	1.773 (2)			Mn–O1	1.790 (3)
Mn1–N11	2.196 (2)	Mn2–N21	2.154 (2)	Mn–N3	2.106 (6)
Mn1–N13	2.166 (3)	Mn2–N23	2.180 (3)	Mn–N5	2.232 (7)
Mn1–N12	2.067 (2)	Mn2–N22	2.047 (2)	Mn–N1	2.051 (6)
Mn1–O11	2.044 (2)	Mn2–O21	2.085 (3)	Mn–O2	2.001 (6)
Mn1–O12	2.083 (2)	Mn2–O22	2.053 (2)	Mn–O3	2.133 (6)
Mn1–O–Mn2	125.1 (1)			Mn–O1–Mn′	125.0 (3)
N11–Mn1–N12	84.1 (1)	N21–Mn2–N22	83.4 (1)	N1–Mn–N3	84.6 (2)
N11–Mn1–N13	82.4 (1)	N21–Mn2–N23	84.9 (1)	N1–Mn–N5	83.1 (2)
N12–Mn1–N13	84.6 (1)	N22–Mn2–N23	83.1 (1)	N3–Mn–N5	84.2 (3)
O11–Mn1–O	96.0 (1)	O21–Mn2–O	95.7 (1)	O1–Mn–O2	96.1 (2)
O11–Mn1–O12	91.9 (1)	O21–Mn2–O22	89.6 (1)	O2–Mn–O3	91.2 (2)
O–Mn1–O12	96.0 (1)	O–Mn2–O22	96.5 (1)	O1–Mn–O3	95.0 (2)
O–Mn1–N12	176.8 (1)	O–Mn2–N22	175.7 (1)	O1–Mn–N1	176.4 (2)
O–Mn1–N13	170.0 (1)	O21–Mn2–N23	169.9 (1)	O2–Mn–N3	171.6 (2)
O–Mn2–N11	169.0 (1)	O22–Mn2–N21	170.0 (1)	O3–Mn–N5	168.1 (2)
O11–Mn1–N11	91.9 (1)	O21–Mn2–N21	91.7 (1)	O2–Mn–N1	87.4 (2)
O11–Mn1–N12	86.6 (1)	O21–Mn2–N22	87.0 (1)	O2–Mn–N5	92.3 (3)
O–Mn1–N11	93.9 (1)	O–Mn2–N21	93.2 (1)	O1–Mn–N3	91.9 (2)
O–Mn1–N13	92.7 (1)	O–Mn2–N23	94.0 (1)	O1–Mn–N5	95.9 (2)
O12–Mn1–N12	85.8 (1)	O22–Mn2–N22	86.8 (1)	O3–Mn–N1	85.8 (2)
O12–Mn1–N13	92.3 (1)	O22–Mn2–N23	92.2 (1)	O3–Mn–N3	90.8 (2)
Ligand Geometry–Acetate Groups					
C31–O11	1.251 (3)	C41–O21	1.249 (4)	C1–O3	1.260 (10)
C31–O21	1.253 (4)	C41–O22	1.252 (3)	C1–O2′	1.241 (8)
C31–C32	1.499 (5)	C41–C42	1.501 (4)	C1–C2	1.491 (14)
O11–C31–O21	125.1 (3)	O12–C41–O22	125.5 (2)	O3–C1–O2′	126.1 (8)
O11–C31–C32	117.7 (3)	O12–C41–C42	117.7 (2)	O3–C1–C2	116.8 (7)
C32–C31–O21	117.2 (3)	C42–C41–O22	116.8 (3)	C2–C1–O2′	117.2 (8)
O11···O21	2.222 (3)	O12···O22	2.223 (3)		

	min	max	mean	min	max	mean
Tri-1-pyrazolylborate Groups[b]						
Mn–N2–N1	119.4 (2)	122.6 (2)	120.8	118.5 (5)	122.0 (4)	120.4
Mn–N2–C3	130.6 (2)	134.8 (2)	133.1	131.8 (5)	136.4 (5)	133.4
N–B–N	109.3 (3)	107.1 (3)	108.2	108.1 (7)	109.3 (6)	108.5
B–N1–C5	130.6 (3)	132.5 (3)	131.3	130.1 (6)	131.5 (6)	130.7
B–N1–N2	119.2 (2)	120.0 (2)	119.5	118.8 (6)	119.4 (5)	119.1
N2–N1–C5	108.5 (3)	109.5 (2)	109.2	108.9 (5)	110.8 (7)	110.1
N1–C5–C4	108.3 (3)	109.2 (2)	108.7	107.0 (7)	109.0 (7)	108.0
C5–C4–C3	104.8 (3)	105.4 (3)	105.1	105.7 (9)	106.1 (7)	105.9
C4–C3–N2	110.0 (3)	111.4 (4)	110.8	108.8 (8)	111.3 (3)	110.0
C3–N2–N1	105.9 (3)	106.9 (2)	106.2	105.1 (7)	106.6 (6)	106.0
B–N1	1.523 (4)	1.550 (4)	1.537	1.526 (9)	1.539 (12)	1.534
N2–N1	1.357 (3)	1.376 (4)	1.365	1.348 (8)	1.367 (7)	1.360
N1–C5	1.333 (4)	1.361 (3)	1.346	1.334 (11)	1.348 (12)	1.341
C5–C4	1.360 (6)	1.372 (5)	1.366	1.353 (15)	1.370 (14)	1.363
C4–C3	1.368 (6)	1.385 (5)	1.378	1.363 (11)	1.406 (11)	1.383
C3–N2	1.328 (5)	1.338 (4)	1.332	1.330 (12)	1.360 (8)	1.342

	min	max	mean	
Solvate Geometry				
C–N	1.033 (8)	1.120 (7)	1.113	1.163 (25)
C–C	1.408 (7)	1.446 (6)	1.422	1.474 (30)
C–C–N	177.7 (6)	179.5 (5)	178.5	180.0 (20)

[a] See Figures 1 and 2 for atom labeling schemes. Numbers in parentheses are esd's in the last digit(s) listed. [b] Pyrazole rings are labeled as described in Table IV of ref 6c.

The features at 400–600 nm of these binuclear Mn(III) compounds can be compared to those of several mononuclear manganese(III) complexes, which exhibit d–d bands in this region with similar molar extinction coefficients.[19] Some of the intensity in the spectrum of **1**, however, is due to charge-transfer transitions within the $\{Mn_2O(O_2CCH_3)_2\}^{2+}$ core, since resonance Raman spectra (vide infra) reveal the ν(Mn–O_2CCH_3) modes ~336–343 cm^{-1} to be enhanced when excited with 457 and 488 nm, compared with 407 nm, laser lines (data not shown). The assignment of charge-transfer bands above 400 nm to the (μ-oxo)bis(μ-acetato)diiron(III) core in **4** was facilitated by comparison with the optical absorption spectrum of $[Fe_2O(H_2B(pz)_2)_2(HB(pz)_3)_2]$,[20]

(19) Dingle, R. *Acta Chem. Scand.* **1966**, *20*, 33.

(20) Armstrong, W. H.; Lippard, S. J., to be submitted for publication.

Table V. Structural Comparisons for Several $\{M_2O(O_2CR)_2\}^{2+}$ Containing Complexes[a]

feature	$1{\cdot}4CH_3CN$[b]	$1{\cdot}CH_3CN$[b]	$4{\cdot}4CH_3CN$[c]	5[d]	6[e]
$M-O_{oxo}$	1.773 (2)	1.790 (3)	1.780 (2)	1.80 (1)	1.781 (4)
	1.787 (2)		1.788 (2)		
M–O–M	125.1 (1)	125.0 (3)	123.6 (1)	117.8 (2)	118.7 (4)
M···M	3.159 (1)	3.175 (1)	3.146 (1)	3.084 (3)	3.063 (2)
$M-O_{acetate}$	2.044 (2)–	2.001 (6)	2.040 (2)–	1.94 (1)	2.041 (6)
	2.085 (3)	2.133 (6)	2.050 (3)	2.05 (1)	2.043 (6)
$M-N_{trans}$[f]	2.067 (2)	2.051 (6)	2.200 (3)	2.06 (1)	2.205 (7)
	2.047 (2)		2.176 (3)		
$M-N_{cis}$[f]	2.196 (2)	2.232 (7)	2.153 (3)	2.25 (2)	2.158 (7)
	2.166 (3)	2.106 (6)	2.159 (3)	2.22 (2)	2.173 (6)
	2.154 (2)		2.150 (3)		
	2.180 (3)		2.148 (3)		

[a] M = Mn (**1**,**5**) or Fe (**4**,**6**). Bond distances are given in Å and angles in deg. [b] This work. [c] Reference 6c. [d] Reference 7. [e] Reference 21. [f] cis and trans refer to position with respect to the M–(μ-oxo) bonds.

Table VI. Electronic Spectral Data for Oxo-Bridged Binuclear Mn(III) and Fe(III) Centers[a]

$[Mn_2O(O_2CCH_3)_2(HB(pz)_3)_2]$ **1**[b]	$[Mn_2O(O_2CCH_3)_2(TACN)_2]^{2+}$ **5**[c]	$[Fe_2O(O_2CCH_3)_2(HB(pz)_3)_2]$ **4**[d]	Mn-catalase *L. plantarum*[e]
283 (6000)		338 (4635)	
385 sh (405)		350 sh (2790)	380 sh (145)
458 sh (165)		457 (505)	470 (135)
486 (210)	486 (337)	492 (460)	485 sh (130)
503 sh (190)			
524 sh (175)	521 (323)	528 sh (165)	
540 sh (165)			
582 sh (95)			
760 (58)	720 (56)	695 (70)	680 (36)
	990 (28)	995 (3.5)	

[a] λ reported in nm, and numbers in parentheses are extinction coefficients per mol of metal atom. [b] This work. [c] Reference 7. [d] Reference 6c. [e] Reference 3a.

which has no intense features in this spectral region. A similar comparison is not possible for high spin d^4 Mn(III) where, unlike high spin d^5 Fe(III), d–d transitions are spin-allowed. The absorption at 760 nm resembles the charge-transfer bands in mononuclear Mn(III) compounds.[19]

Although a discrete band was observed at 990 nm (ϵ 28) in **5** and at 995 nm (3.5) in **4**, we see no resolved peak in this region for **1** or **2**, only a broad tail from the peak at 760 nm (Figure 3). This tail extends to 1200 nm and has a molar absorptivity of 25 at 1000 nm. The origin of this near infrared transition is uncertain.

Infrared and Resonance Raman Spectroscopy. Table VII summarizes the principal infrared and Raman vibrational frequencies and proposed mode assignments for **1**. The spectra and their interpretation are nearly identical with those previously reported for the iron analogue **4**. Conspicuous features in the infrared spectrum are the B–H stretching band at 2479 cm^{-1} (see Experimental Section), the carboxylate bridges as broad, intense peaks at 1580 (1560 for **6**) (ν_{as}(OCO)) and 1410 cm^{-1} (ν_s(OCO)), and a series of sharp, intense peaks for the pyrazole rings at 1500–600 cm^{-1}. A broad, asymmetric peak of low intensity is centered ~540 cm^{-1}. It has a half-width of ~50 cm^{-1} and contains two or more components. One of these occurs at ~560 cm^{-1} and is assigned to the Mn–O–Mn symmetric stretching mode, ν_s, based upon the appearance of a strong band at ~558 cm^{-1} (Table VII) in the resonance Raman spectra of solid **1** obtained with 4067-Å Kr^+ laser excitation. As shown in Figure 4 for **2**, this band shifts to 541 cm^{-1} upon ^{18}O exchange, confirming its assignment to ν_s. The magnitude of the isotopic shift for this band (17 cm^{-1}) is consistent with those of the analogous ν_s(Fe–O–Fe) stretches at 528 cm^{-1} in **4** and 540 cm^{-1} in **6**; upon $^{18}O \rightarrow {}^{16}O$ exchange this mode shifts to 511 cm^{-1} in **4** and 523 cm^{-1} in **6**.[6c,21]

The Fe–O–Fe and Mn–O–Mn asymmetric stretches, ν_{as} in **4** and **1**, are buried beneath ligand vibrations in the region 700–800 cm^{-1}. This mode occurs at 751 cm^{-1} for **4**[6c] and 749 cm^{-1} for **6**,[21] as determined from their $^{18}O-{}^{16}O$ difference Fourier transform IR spectra. This assignment has been confirmed by recent reexamination of the RR spectrum of solid **4** at low temperatures,[22]

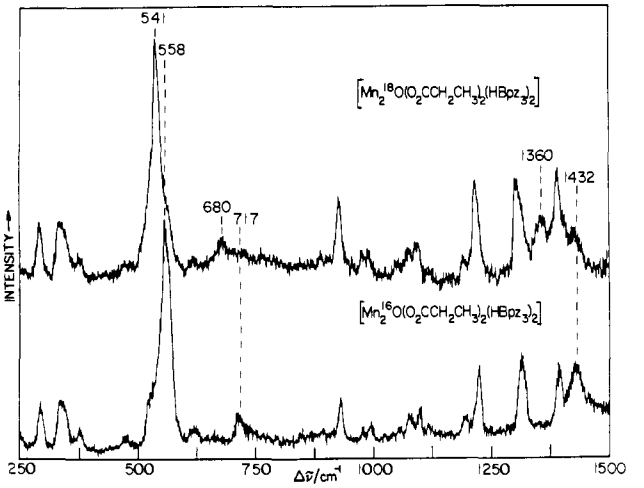

Figure 4. Resonance Raman spectra of **2** and ^{18}O-**2** obtained via backscattering in KCl pellets at 77 K by using 4067-Å Kr^+ laser excitation and 8-cm^{-1} slit widths.

in which the ν_{as} (Fe–O–Fe) mode shifts from 755 cm^{-1} (^{16}O) to 721 cm^{-1} (^{18}O) upon isotopic exchange. As indicated in Figure 4, the analogous ν_{as} (Mn–O–Mn) stretch can be located at 717 cm^{-1} in the RR spectrum of **2** via its similarly large (37 cm^{-1}) $^{18}O \rightarrow {}^{16}O$ isotopic shift. This assignment is further supported by a Raman band at 1432 cm^{-1}, which shifts to 1360 cm^{-1} in the ^{18}O spectrum. The 1432-cm^{-1} frequency is ~$2\nu_{as}$ (717 cm^{-1}) and, because it is ^{18}O-sensitive, is identifiable as the first overtone of the asymmetric Mn–O–Mn stretch. This overtone is expected to be highly Raman active from symmetry considerations ($B_2 \times B_2 = A_1$). A similarly strong $2\nu_{as}$ (Fe–O–Fe) is observed at 1504 cm^{-1} in the RR spectrum of solid **4**.[22]

The assignment of the 558 (ν_s) and 717 cm^{-1} (ν_{as}) Raman bands is further substantiated by a simple valence force field normal

(21) Spool, A.; Williams, I. D.; Lippard, S. J. *Inorg. Chem.* **1985**, *24*, 2156.

(22) Czernuszewicz, R. S.; Sheats, J. E.; Spiro, T. G. *Inorg. Chem.*, in press.

Table VII. Observed Infrared and Raman Spectral Bands and Proposed Assignments for $[Mn_2O(O_2CCH_3)_2(HB(pz)_3)_2]$ (**1**)

IR[a]	RR[b]	assignment[c]
166 vw	168	
178 w	179 w	deformation
205	206	modes, δ
235		
248		
272	271	ν(Mn–N)
288 sh	293	
298		
334 sh	336	
340	343 sh	ν(Mn–O_2CR)
364	361 sh w	
379	378	
540		
559 br, sh	558 s (17)[d]	ν_s(Mn–O–Mn)
617	618	
659		L
666 sh	667 w	L
712	717 (37)	ν_{as}(Mn–O–Mn)
725 sh	730 sh	
	742 vw	
789 w	793 vs	
881 w	870 br, w	
928 w	929	
987	990	
1047 s	1053	
1070	1072	L
1091 w	1096	
	1159	
	1187	
1212	1220	
1311	1311	
1391	1391	
1407 s	1407 sh	
	1432 (72)	$2\nu_{as}$(Mn–O–Mn)[e]
	1442 sh	L
1504	1482	L
1511 sh		
1580 s		ν_{as}(OCO)

[a] Far-IR spectra (100–600 cm^{-1}) in Nujol mulls, held between polyethylene disks, obtained with a Digilab FTIR spectrometer. Mid-IR spectra (600–1500 cm^{-1}) in KBr pellet. [b] Resonance Raman (RR) in KCl pellets kept at liquid N_2 temperature. Symbols: s, strong; w, weak; sh, shoulder; br, broad. [c] ν = stretch, ν_s = symmetric stretch, ν_{as} = asymmetric stretch, δ = deformation, L = assigned as vibration of $HB(pz)_3$. [d] Parentheses indicate the $^{18}O \rightarrow {}^{16}O$ isotopic shift upon change with $H_2{}^{18}O$. [e] Overtone.

mode calculation,[23] as described previously.[6c,21] The stretching and interaction force constants are k_d = 3.34 mdyn/Å and k_{dd} = 0.74 mdyn/Å, respectively. From these constants we compute ν_s = 539 cm^{-1} and ν_{as} = 681 cm^{-1} for [^{18}O]-**1**, which are identical within experimental error to the measured values of 541 (ν_s) and 680 (ν_{as}) cm^{-1}.

The three Raman and IR bands in the 275–375-cm^{-1} region are not sensitive to the isotopic exchange of the μ-oxo bridge and are assigned to the Mn–N (271 cm^{-1}) and manganese–carboxylate oxygen (~340 cm^{-1}) modes, by analogy to the comparable bands in the spectrum of **4**. These and other modes are listed in Table VII along with their suggested assignments.

Magnetic Susceptibility. Magnetic studies of powdered samples of **1**·CH_3CN and **1**·4CH_3CN were carried out in two different laboratories.[1d,f] Temperature dependent molar susceptibilities and effective magnetic moments per Mn for these two studies are listed in Tables S5 and S6. Both sets of results are consistent with two isolated high spin Mn(III) centers with only weak antiferromagnetic exchange coupling between them. Plots of χ_M^{-1} vs. T for both **1**·CH_3CN (not shown) and **1**·4CH_3CN (Figure 5) samples increase nearly linearly with temperature. The magnetic moment of the sample of **1**·CH_3CN decreased slightly from 4.96 to 4.88 μ_B per Mn between 300 and 15.7 K and further decreased to 4.61 μ_B at 5.4 K. It is possible that the decrease in the moment below 15.7 K can be attributed to zero-field splitting of the Mn(III) ground state.[24] The absence of ESR resonances at 10 GHz indicates that the principal zero-field splitting parameter, D, is greater than 0.33 cm^{-1}. The magnetic moment of the **1**·4CH_3CN sample was measured to be 4.89 μ_B per manganese at 278 K, decreasing to 4.77 μ_B at 100 K, 4.43 μ_B at 20 K, and finally to 4.03 μ_B at 6.01 K. At present we have no explanation for the small differences between the two sets of results. Attempts to fit the χ_M^{-1} vs. T data to the expression derived from the spin-exchange Hamiltonian $\mathcal{H}' = -2JS_1 \cdot S_2$ for $S_1 = S_2 = 2$[25] led to J values ~ −0.2 to −0.7 ± 0.1 cm^{-1}, but in neither case was it possible to obtain a good simulation over the entire temperature range.

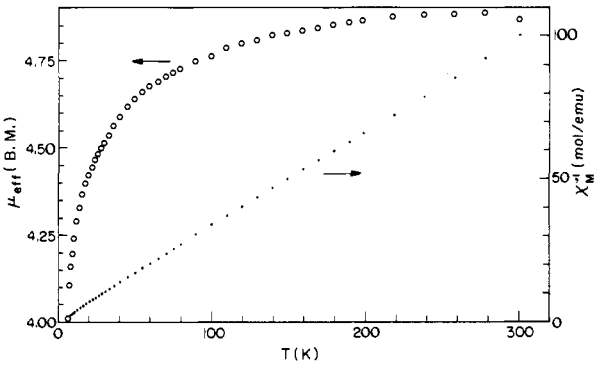

Figure 5. Plots of χ_M^{-1} and μ_{eff} vs. T for $[Mn_2O(O_2CCH_3)_2(HB(pz)_3)_2]$.

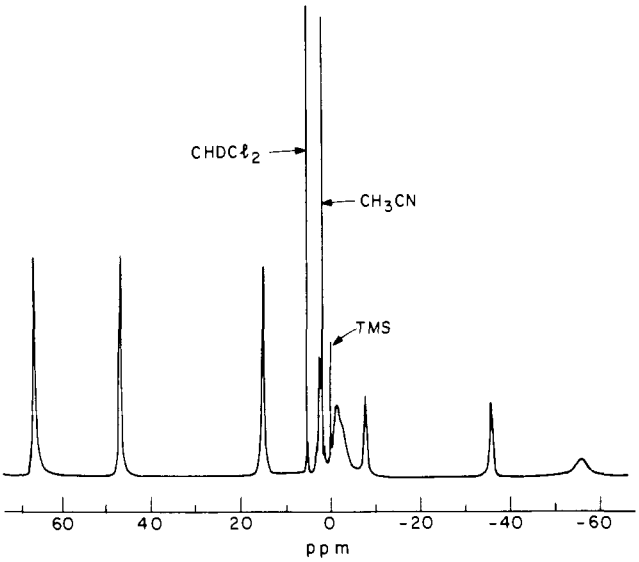

Figure 6. 250-MHz proton NMR spectrum of $[Mn_2O(O_2CCH_3)_2(HB(pz)_3)_2]$·4$CH_3CN$ in CD_2Cl_2.

The absence of appreciable magnetic exchange coupling between Mn(III) centers in **1** and its TACN analogue **5**, which has a reported value of 5.12 μ_B per Mn,[7] is very different behavior from that of the more strongly antiferromagnetically coupled (J = −121 cm^{-1}), isostructural iron(III) compound **4**, $[Fe_2O(O_2CCH_3)_2(HB(pz)_3)_2]$.[6c] These differences are also manifest by the much greater effective magnetic moment of **1** at 295 K in CD_2Cl_2 or $CDCl_3$ solutions, 4.92 μ_B by the Evans method,[15] compared with 1.71 μ_B for compound **4**. As mentioned above, the d_{z^2} orbitals directed along the M–O_{oxo} bond vectors are occupied in the high spin d^5 Fe(III) compound **4** but are unoccupied in the high spin d^4 Mn(III) analogues. This difference eliminates a major pathway for orbital coupling in **1** compared with **4** and leads to a markedly diminished magnetic exchange interaction,

(23) (a) Wing, R. M.; Callahan, K. P. *Inorg. Chem.* **1969**, *8*, 871. (b) Cotton, F. A.; Wing, R. M. *Inorg. Chem.* **1965**, *4*, 867.

(24) Kennedy, B. J.; Murray, K. S. *Inorg. Chem.* **1985**, *24*, 1552.
(25) O'Connor, C. J. *Prog. Inorg. Chem.* **1982**, *29*, 203.

the consequences of which on the NMR spectra of these molecules are discussed below.

Proton NMR Spectroscopy. Manganese(III) is a favorable paramagnetic transition-metal ion for observing ligand proton resonances,[26] and the spectra of **1–3** were no disappointment. As shown in Figure 6, the proton NMR spectrum of $[Mn_2O(O_2CCH_3)_2(HB(pz)_3)_2]$ consists of eight identifiable resonances in the range $+67 > \delta > -56$ ppm. By contrast, the spectrum of the iron(III) analogue **4** is fully contained in the $+13 > \delta > +3$ ppm chemical shift range. The wider chemical shift range for **1–3** is due chiefly to the larger magnetic moment of the manganese(III) complex. Consider, for example, the methyl protons of the bridging acetate groups, which occur at 10.5 ppm in the iron complex **4** and at 65.6 ppm in the Mn(III) complex **1**. This assignment is made by comparing the results for $[Mn_2O(O_2CCH_3)_2(HB(pz)_3)_2]$ with those for $[Mn_2O(O_2CCD_3)_2(HB(pz)_3)_2]$ (Table VIII). The major difference in methyl group isotropic shifts for compounds **1** and **4** can be understood from the theory of exchange coupled binuclear complexes.[27] Assuming that dipolar contributions to the proton shifts are negligible, the ratio $(\Delta H_{Mn}/\Delta H_{Fe})$ will to a first approximation depend upon the ratio of molar susceptibilities, χ_{Mn}/χ_{Fe}, or equivalently, $[\mu_{eff}^2(Mn)/\mu_{eff}^2(Fe)]$. The latter value at room temperature for solutions of **1** and **4** in CD_2Cl_2 is 8.28, which is within 8% of the $(\Delta H_{Mn}/\Delta H_{Fe})$ ratio of $(65.6 - 2.1)/(10.5 - 2.1) = 7.6$. In the propionate-bridged complex **2**, the chemical shift of the CH_2 protons is similarly shifted downfield to 65.4 ppm, whereas the methyl group resonates at 6.2 ppm (Table VIII), reflecting the usual attenuation of the Fermi coupling constant A with distance from the paramagnetic center.

The resonance at −1.2 ppm in **1** was assigned to the B–H proton of the hydrotris(1-pyrazolyl)borate group by comparison with the spectrum of the deuteriated (B–D) derivative (Table VIII). The remaining two groups of these resonances occur in an intensity ratio of 4:2 and are assigned as pyrazolyl ring proton cis and trans to the μ-oxo group, respectively. These resonances are preserved in complexes **1–3**. As shown schematically below, the protons

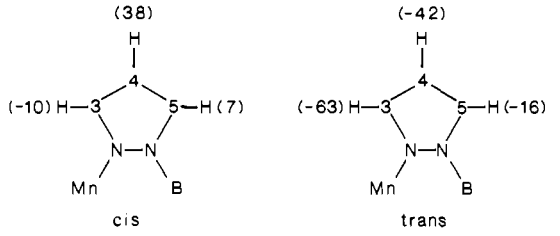

of the trans pyrazolyl ring are all shifted upfield from their chemical shift values in the free ligand while two of three protons on the cis pyrazolyl rings are shifted downfield and one is shifted upfield. This reversal in sign of the net shift for cis vs. trans pyrazolyl ring protons is consistent with the difference in d-orbital σ electron density for high spin d^4 Mn(III) discussed above.[28] Protons on the pyrazolyl rings cis to the μ-oxo group experience both σ and π electron density effects, whereas those on the trans pyrazolyl rings are influenced only by d_π electrons.

The assignment of the H(3) ring protons was made on the basis of their being consistently broader (770–1000 Hz) by a factor of 5–7 than resonances assigned to H(4) and H(5) (Table VIII). Greater line width is expected on the basis of dipolar relaxation for protons closest to the paramagnetic manganese centers ($\propto R^{-3}$), and a similar argument was used to assign the pyrazolyl H(3) protons in the iron analogue **4**.[6c] Consistent with this analysis is the fact that the protons of the formate groups in **3** are even

Table VIII. Proton NMR Data at 25 °C for Compounds **1–4**[a]

	chemical shifts (ppm) and relative intensities									
				pyrazolylborate						
				cis to oxo			trans to oxo			
compound	BH	bridging carboxylate		H3	H4	H5	H3	H4	H5	
$[Mn_2O(O_2CCH_3)_2(HB(pz)_3)_2]$	−1.2 (2)	65.6 (6, 170)		−2.4 (4, br)	46.2 (4, 130)	14.3 (4, 130)	−54.9 (2, 670)	−34.9 (2, 200)	−8.3 (2, 180)	
$[Mn_2O(O_2CCD_3)_2(HB(pz)_3)_2]$	−1.0 (2)			−2.5 (4, br)	46.2 (4, 180)	14.3 (4, 170)	−54.9 (2, 540)	−34.9 (2, 210)	−8.3 (2, 230)	
$[Mn_2O(O_2CCH_3)_2(DB(pz)_3)_2]$		65.9 (6, 210)		−2.4 (4, 770)	46.3 (4, 150)	14.3 (4, 150)	−54.9 (2, br)	−35.1 (2, 250)	−8.3 (2, 250)	
$[Mn_2O(O_2CCH_2CH_3)_2(HB(pz)_3)_2]$	−1.0 (2)	65.4 (CH_2) (4, 180)	6.2 (CH_3) (6, 90)	−2.5 (4, br)	46.4 (4, 130)	14.5 (4, 130)	−56.0 (2, 670)	−35.3 (2, 180)	−7.8 (2, 180)	
$[Mn_2O(O_2CH)_2(HB(pz)_3)_2]$	0.0 (2)	−1 (2, >1500)		−3.0 (4)	44.3 (4)	13.0 (4)	−50.0 (2)	−31.3 (2)	−9.7 (2)	
$[Fe_2O(O_2CCH_3)_2(HB(pz)_3)_2]^b$	3.0	10.5								

[a] Data are presented as chemical shifts in ppm vs Me_4Si. Positive shifts are downfield from Me_4Si. Numbers in parentheses are relative intensity and full width at half-height in Hz., respectively; br = broad. [b] Data from ref 6c.

(26) Swift, T. J. In *NMR of Paramagnetic Molecules*; LaMar, G. N.; Horrocks, W. deW., Jr., Holm, R. H., Eds.; Academic Press: New York, 1973; pp 79–81.

(27) LaMar, G. N.; Eaton, G. R.; Holm, R. H.; Walker, F. A. *J. Am. Chem. Soc.* **1973**, *95*, 63 and references cited therein.

(28) See, for example: the discussion by Horrocks, W. DeW., Jr. In *NMR of Paramagnetic Molecules*; LaMar, G. N., Horrocks, W. deW., Jr., Holm, R. H., Eds.; Academic Press: New York, 1973; p 128.

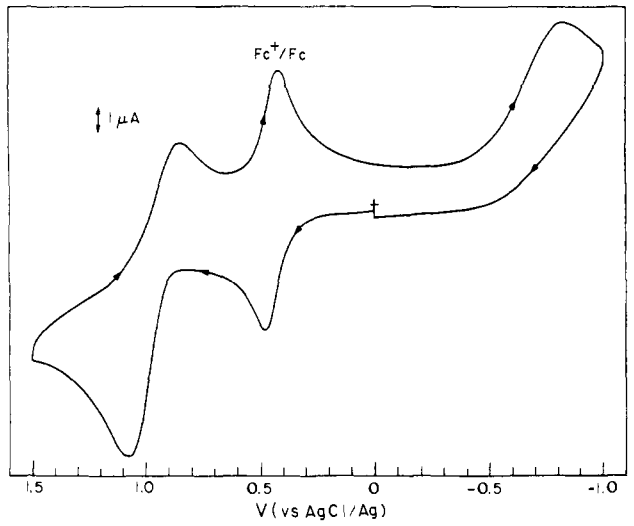

Figure 7. Cyclic voltammogram of $[Mn_2O(O_2CCH_3)_2(HB(pz)_3)_2]$ at 200 mVs^{-1} at a platinum disk electrode in CH_3CN with 0.1 M (n-Bu_4N)(ClO_4) as supporting electrolyte, referenced to AgCl/Ag.

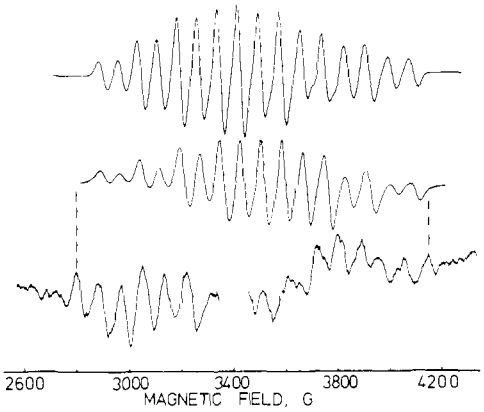

Figure 8. (Bottom): electron spin resonance (ESR) spectrum of spinach photosystem II particles illuminated at 300 K and frozen to 10 K. (Middle): ESR spectrum at 100 K of **2** in CH_2Cl_2 oxidized by air in a two-phase aqueous mixture. (Top): simulation of oxidized **2** by using the parameters A_1 = 77 G, A_2 = 159 G, intrinsic line width = 25 G, intrinsic line width = 25, linear M_1 line width coefficient, a_1 = 6.0 G, a_2 = 2.0 G. See ref 5b for further details of the simulation.

broader (>1500 Hz), while the methyl protons of the bridging propionate groups in **2** are narrower (90 Hz). The distance (R) of the formate protons from the Mn ions is ~3.8 Å, whereas R = 3.5 Å for the H(3) ring protons, and R > 4.8 for the propionate methyl protons. Assignment of the remaining two resonances to the H(4) and H(5) protons is less straightforward and a definitive choice is not apparent. The tentative assignments indicated in the above diagrams and in Table VIII were made arbitrarily.

As can be seen by the foregoing discussion, the $\{Mn_2O(O_2CR)_2\}^{2+}$ core exhibits highly paramagnetically shifted, relatively narrow proton NMR spectra which should greatly facilitate the identification and study of this and related dimanganese(III) cores in biology.

Electrochemistry and Electron Spin Resonance Spectroscopy. A cyclic voltammogram of **1** in acetonitrile with tetra-*n*-butylammonium perchlorate as supporting electrolyte (Figure 7) displays a quasi-reversible one-electron oxidation with $E_{1/2}$ = 0.51 V vs. internal Fc^+/Fc, corresponding to formation of the Mn_2(III,IV) mixed valence complex and an irreversible reduction at −1.20 V. Similar behavior was reported for $[Mn_2O(O_2CCH_3)_2(TACN)_2]^{2+}$, **5**,[7] and a $[Mn_2O(O_2CCH_3)_2(TACN)_2]^{3+}$ mixed valence Mn_2(III,IV) complex has recently been crystallized and structurally characterized.[29] The irreversible reduction potential for **1** is ~0.7 V more negative than for **5**, however. Further studies detected another quasi-reversible wave at $E_{1/2}$ = +1.22 V vs. Fc^+/Fc, presumably corresponding to the Mn_2(III,IV)/Mn_2(IV,IV) couple. These results are reminiscent of the $[Mn_2O_2(phen)_4]^{n+}$ system,[5a,30a] for which $E_{1/2}$ values (converted vs. the Fc^+/Fc reference electrode) of +0.25 and +1.17 V are reported for Mn_2(III,III)/Mn_2(III,IV) and Mn_2(III,IV)/Mn_2(IV,IV) redox couples, respectively.

It was also possible to generate a mixed valence complex by oxidation of **1** in air or by $KMnO_4$ in a two-phase aqueous methylene chloride mixture.[30b] The frozen solution (T = 100 K) electron spin resonance spectrum of the mixed valence complex of **2** exhibited a 16 line pattern centered at g = 2.0 with a width of 1180 G, as shown in Figure 8. The spectrum is essentially identical with those found for the cations $[Mn_2O_2(bpy)_4]^{3+}$ and $[Mn_2O_2(phen)_4]^{3+}$.[5b] A simulation based upon the same spin Hamiltonian used successfully to predict the spectra of these cations is also given in Figure 8. Agreement between the theoretical and experimental spectra is found for the ^{55}Mn hyperfine parameters: A_1 = 77 and A_2 = 159 G, indicating little hyperfine anisotropy and a trapped valence state consistent with Mn(III) and Mn(IV). The equivalent hyperfine constants for the monomeric ions[5b] are $|A[Mn(III)]|$ = 80 and $|A[Mn(IV)]|$ = 77 G. The intensity of the ESR signal created by oxidation with $KMnO_4$ was found to be the same as that for the signal from the purified mixed valence complexes $[Mn_2O_2(phen)_4](ClO_4)_3 \cdot CH_3COCH_3$ and $[Mn_2O_2(bpy)_4](ClO_4)_3 \cdot 2H_2O$ in CH_3CN. Also, the temperature dependence of the intensity between 6 and 50 K established that the ESR signal arises from the ground state. These results indicate that the signal originates from the $S = {}^1/_2$ state and that antiferromagnetic coupling occurs between the Mn ions in oxidized **2** with J comparable to that for the di-μ-oxo complexes ($J \sim -130$ to -150 cm^{-1}).[5b] Attempts to isolate and purify the mixed valence complex are in progress.[30a]

The ESR spectrum of the mixed valence complex displays a hyperfine structure similar to that for one of the forms of the manganese center of the photosynthetic water oxidizing complex in spinach when formed in the S_2 oxidation state by multiple turnovers under illumination at room temperature (see Figure 8). This photochemically generated species exhibits a 16-line spectrum with larger average splitting than observed for the mixed valence form of **2** and is attributed to a mixed valence state of a binuclear manganese center.[31] The spectral and thermal behavior of the binuclear complexes does not mimic that of the more complex 19-line ("multiline") spectrum produced in the S_2 state by single turnover illumination of the water-oxidizing complex, which has been ascribed to a tetranuclear manganese species.[2a,b,32] The ability of various mixed valence dimanganese complexes to mimic this spectrum results from the near constancy of the ^{55}Mn hyperfine coupling constants for various coordination geometries and ligand types possessing O or N donor atoms of comparable covalency.

The substantial increase in redox potential in going from Mn_2(III,III)/Mn_2(III,IV) at 0.51 V to the putative Mn_2(III,IV)/Mn_2(IV,IV) couple at 1.22 V (vs. Fc^+/Fc) indicates that these complexes do not model very well the redox potential for the oxidation step of the enzyme presumed to coincide with the latter couple, either the S_2–S_3 transition or the S_3–S_4 transition. While the exact potentials of these equilibria are not known, they have an upper limit of ~0.95 V set by the potential of the primary chlorophyll photooxidant (P680). Thus, there must exist a mechanism within green plants to suppress the large increase in reduction potential for manganese that is observed upon successive oxidations in model complexes. Charge neutralization within the active site core, perhaps by proton release or uptake of Cl^-, might

(29) Wieghardt, K.; Bossek, U.; Girerd, J. J.; Bonvoisin, J.; Beauvillain, P.; Weiss, J.; Nuber, B.; Heinze, J. *Angew. Chem.* **1986**, *98*, 1026.

(30) (a) Morrison, M. M.; Sawyer, D. T. *J. Am. Chem. Soc.* **1977**, *99*, 257. (b) Note Added In Proof: Resonance Raman and mass spectrometric studies have recently shown this species to be $[(HB(pz)_3)Mn(O)_2(O_2CCH_3)Mn(HB(pz)_3)]$ (Sheats, J. E.; VnniNair, B. C.; Petrouleas, V.; Artandi, S.; Dismukes, G. C., to be submitted for publication.

(31) Dismukes, G. C. In *Manganese in Metabolism and Enzyme Function*; Schram, V. L., Wedler, F. C., Eds.; Academic Press: New York, 1986; p 275.

(32) Dismukes, G. C.; Ferris, K.; Watnick, P. *Photobiochem. Photobiophys.* **1982**, *31*, 243.

provide the requisite adjustment in redox potential.

Summary and Conclusions. The manganese(III) analogues of the iron(III) hemerythrin model complexes, $[Mn_2O(O_2CR)_2(HB(pz)_3)_2]$, have been synthesized and characterized in this study. The major differences between the two classes of molecules derive from removal of a d-electron on each metal center from the d_{z^2} orbital directed along the metal-μ-oxo vectors in going from the d^5-d^5, Fe_2(III,III) to the d^4-d^4, Mn_2(III,III) system. The consequences of this change in electronic structure are manifest in differences in the metal-ligand bond lengths trans to the bridging oxygen atom and, more importantly, a markedly diminished antiferromagnetic spin exchange interaction in the dimanganese complex. The greater paramagnetism and faster spin relaxation of the latter leads to relatively sharp, contact-shifted ligand proton resonances in the NMR spectrum that will be valuable in identifying dimanganese centers of this kind in biology. Moreover, these results suggest that substitution of Mn(III) for Fe(III), if it could be experimentally achieved in proteins containing the $\{Fe_2O\}^{4+}$ core, would be a powerful way to probe the nature of these centers in iron-oxo proteins such as ribonucleotide reductase.

Acknowledgment. This work was supported by research grants from the National Institutes of Health General Medical Institute GM-32134 (to S.J.L.) and the National Science Foundation CHE82-17920 (to G.C.D.). Additional support is acknowledged by G.C.D. for an Alfred P. Sloan Foundation Fellowship, by J.E.S. for a faculty research fellowship from Rider College, by J.S. for an NIH Research Career Development Award AM-01222, by W.H. Armstrong from NCI Training Grant CA-09112, and by G.C.D. and V.P. for a NATO travel grant (236/83). We thank the Biomedical Research Support Shared Instrumentation grant program, Division of Research Resources, for funds to purchase the X-ray diffraction equipment (at MIT), NIH Grant RR-02243, Dr. J. C. Dewan for obtaining the low-temperature X-ray data, P. N. Turowski for obtaining spectroscopic data, and S. Artandi for assistance with synthesis. Magnetic data were taken at the Francis Bitter National Magnet Laboratory which is supported by the National Science Foundation.

Note Added in Proof. Resonance R and mass spectrometric studies have recently shown this species to be $[(HB(pz)_3)Mn(O)_2(O_2CCH_3)Mn(HB(pz)_3)]$ (Sheats, J. E.; Unni Nair, B. C.; Petrouleas, V.; Artandi, S.; Dismukes, G. C., to be submitted for publication).

Supplementary Material Available: Tables of thermal and hydrogen atom positional parameters for both $1{\cdot}4CH_3CN$ and $1{\cdot}CH_3CN$ and temperature dependent magnetic susceptibility data for the two compounds as separately measured at MIT and in Athens (6 pages); tables reporting observed and calculated structure factors for $1{\cdot}4CH_3CN$ and $1{\cdot}CH_3CN$ (24 pages). Ordering information is given on any current masthead page.

Relative Metal–Hydrogen, –Oxygen, –Nitrogen, and –Carbon Bond Strengths for Organoruthenium and Organoplatinum Compounds; Equilibrium Studies of $Cp^*(PMe_3)_2RuX$ and (DPPE)MePtX Systems

Henry E. Bryndza,*[1] Lawrence K. Fong,[2] Rocco A. Paciello,[2] Wilson Tam,[1] and John E. Bercaw*[2]

Contribution No. 4056 from the Central Research and Development Department of the E. I. DuPont de Nemours & Co., Inc., Experimental Station, Wilmington, Delaware 19898, and Contribution No. 7397 from the California Institute of Technology, Pasadena, California 91125.
Received April 18, 1986

Abstract: A series of ruthenium, $Cp^*(PMe_3)_2RuX$ ($Cp^* = \eta^5$-C_5Me_5), and platinum, (DPPE)MePtX (DPPE = $Ph_2PCH_2CH_2PPh_2$), compounds have been prepared. The equilibria $L_nM{-}X + H{-}Y \rightleftharpoons L_nM{-}Y + H{-}X$ (L_nM = (DPPE)MePt or $Cp^*(PMe_3)_2Ru$; X, Y = hydride, alkoxide, hydroxide, amide, alkyl, alkynyl, hydrosulfide, cyanide) have been examined. A lower limit of the Ru–N bond strength has been estimated by analysis of the kinetics of the thermal decomposition of $Cp^*(PMe_3)_2RuNPh_2$. The equilibrium constants allow for the determination of relative M–X, M–Y bond dissociation energies (BDEs) for each series of compounds. A linear correlation of L_nM–X to H–X BDEs is found for the two dissimilar metal centers. The generality to other systems and predictive value of this correlation are discussed.

Despite the widespread use of organometallic catalysts to effect homogeneous organic transformations, little is known about the thermochemistry of individual steps comprising catalytic cycles. Recent advances have led to values for some metal–hydrogen and metal–carbon bond strengths,[3] but the factors governing the reactivity of transition metal–heteroatom bonds (M–X: X = OH, OR, NR_2, PR_2, SiR_3, and SH) have been left relatively unexplored.

Early transition metal–oxygen and –nitrogen bonds are quite robust, presumably due to ligand-to-metal π-donation of an oxygen or nitrogen lone electron pair to an empty orbital of the electrophilic metal center.[4] In contrast, there has been a common perception that late transition metal–nitrogen and –oxygen linkages are intrinsically weak due to the mismatch of hard ligand base with soft metal acid,[5] thus explaining the relative scarcity of such complexes in the literature. Only recently has the reaction

(1) E. I. DuPont de Nemours & Company, Inc. Central Research and Development Department.
(2) California Institute of Technology.
(3) For leading references see: (a) Connor, J. A. *Top. Curr. Chem.* **1977**, *71*, 71. (b) Halpern, J. *Acc. Chem. Res.* **1982**, *15*, 238. (c) Pearson, R. G. *Chem. Rev.* **1985**, *85*, 41. (d) Halpern, J. *Inorg. Chim. Acta* **1985**, *100*, 41. (e) Martinho Simoes, J. A.; Beauchamp, J. L. *Chem. Rev.*, *in press*.
(4) Connor, J. A. *Top. Curr. Chem.* **1977**, *71*, 71.
(5) (a) Pearson, R. G. *J. Am. Chem. Soc.* **1963**, *85*, 3533. (b) Pearson, R. G. *J. Chem. Educ.* **1968**, *45*, 643.

0002-7863/87/1509-1444$01.50/0